Environmental Science & Technology

pubs.acs.org/est

Article

Nitrogen Enrichment during Soil Organic Matter Burning and Molecular Evidence of Maillard Reactions

William Bahureksa, Robert B. Young, Amy M. McKenna, Huan Chen, Kevin A. Thorn, Fernando L. Rosario-Ortiz, and Thomas Borch*

Cite This: *Environ. Sci. Technol.* 2022, 56, 4597−4609

Read Online

ACCESS | Metrics & More | Article Recommendations | Supporting Information

ABSTRACT: Wildfires in forested watersheds dramatically alter stored and labile soil organic matter (SOM) pools and the export of dissolved organic matter (DOM). Ecosystem recovery after wildfires depends on soil microbial communities and revegetation and therefore is limited by the availability of nutrients, such as nitrogen-containing and labile, water-soluble compounds. However, SOM byproducts produced at different wildfire intensities are poorly understood, leading to difficulties in assessing wildfire severity and predicting ecosystem recovery. In this work, water-extractable organic matter (WEOM) from laboratory microcosms of soil burned at discrete temperatures was characterized by ultrahigh-resolution Fourier transform ion cyclotron resonance mass spectrometry to study the impacts of fire temperature on SOM and DOM composition. The molecular composition derived from different burn temperatures indicated that nitrogen-containing byproducts were enriched with heating and composed of a wide range of aromatic features and oxidation states. Mass difference-based analysis also suggested that products formed during heating could be modeled using transformations along the Maillard reaction pathway. The enrichment of N-containing SOM and DOM at different soil burning intensities has important implications for ecosystem recovery and downstream water quality.

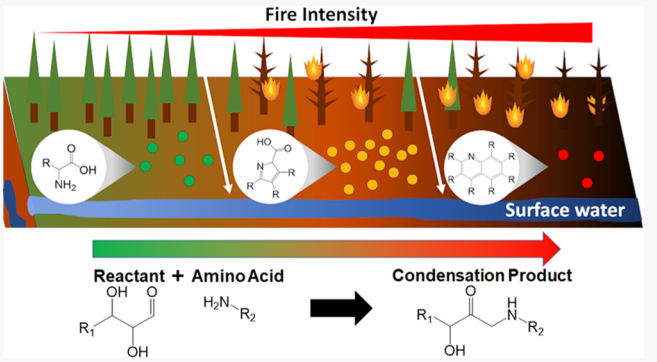

KEYWORDS: *nitrogen, FT−ICR MS, soil organic matter, pyrogenic organic matter*

INTRODUCTION

The 2020 wildfire season was the worst wildfire season to date for many regions around the world, including the western United States, which burned approximately 10 million acres,[1,2] and Australia, which was devastated with over 40 million acres burned.[3] Wildfires are predicted to increase globally,[4−7] threatening forested watersheds responsible for supplying drinking water[8−10] to 180 million people in the western United States[11] and many more abroad.[12−14] Alteration of the soil organic matter (SOM) present will adversely affect both water quality downstream and soil properties for years after the fire has subsided.[9,15−20] Therefore, understanding how wildfires alter SOM composition following fires is of great interest.

The extent of thermal transformation and loss of SOM, known as burn severity, is commonly assessed by comparing bulk prefire SOM, vegetation, and soil properties to postfire features, including soil microbial communities.[21] Importantly, recovery and revegetation depend on the presence of labile, water-soluble nutrients, such as nitrogen.[22] Nitrogen is a limiting reactant for soil microbial productivity,[23] and soil carbon-to-nitrogen (C/N) ratios inversely correlate with SOM reactivity during microbial metabolism.[24,25] Above 200 °C, wildfires can volatilize, transform, and mobilize organic nitrogen,[26] which then leaches from the organic soil layer as water passes through the soil as dissolved organic nitrogen.[27,28] Charred particulate and water-soluble organic matter will be transported downstream from fire-affected watersheds,[29] negatively impacting water quality and even producing toxic effects.[30] Furthermore, the increased formation of toxic nitrogen-containing disinfection byproducts (DBPs) has been observed during drinking water treatment downstream of burned areas.[31−33] Therefore, the molecular composition of charred, water-soluble nitrogen species formed during wildfires is of great interest for the recovery of fire-affected watersheds and water quality studies.

Several reviews summarize the effects of fire intensity on SOM quantity and quality under both laboratory and field conditions, defining fire intensity as a "specific heating temperature over a fixed interval of time below the soil

Received: October 6, 2021
Revised: February 24, 2022
Accepted: February 25, 2022
Published: March 9, 2022

surface".[34] In brief, heating between 200 and 250 °C results in the transformation of biomolecules with concurrent formation of aliphatic, alcohol, carbonyl, and aromatic functionalities, as reported by nuclear magnetic resonance (NMR) spectroscopy.[35−39] Carbonization toward more graphitic structures has been observed around 300 °C, followed by the near total consumption of SOM and formation of a highly condensed aromatic material, often discussed as "dissolved black carbon" when referring to the water-soluble fraction.[36,40,41] Recent models suggest that thermally altered SOM species contain considerable substitution of aromatic rings with nitrogen (including "dissolved black nitrogen"),[42] oxygen, and sulfur species.[43]

Targeted methods have also been applied to study specific constituents that comprise fire-affected SOM. Residues released by biomolecular components and known pyrolysis products of biomolecules, known as biomass burning markers,[44] have been previously studied using pyrolysis[19,45−49] and derivatization[50−52] prior to gas chromatography mass spectrometry, and using liquid chromatography−mass spectrometry.[53,54] The precise identity of many charred residues remains elusive, including nitrogen-containing heterocyclic residues (e.g., pyridines, pyrazines, and pyrrole structures). These residues can resemble melanoidins[42,55,56] which typically form through a cascade of reactions associated with the heating of polysaccharides and proteins, referred to as the Maillard reaction pathway.[57] Melanoidin and intermediate Maillard reaction products (MRPs) are frequently discussed as a pathway for both carbon and nitrogen sequestration following heating in soils[36,58−61] and may therefore describe nutrient sources in postwildfire ecosystems.[62,63] Direct measurement of this pathway has not yet been conducted in charred SOM and would require ultrahigh resolution to probe changes to individual residues associated with the transformation of SOM.

Fourier transform ion cyclotron resonance mass spectrometry (FT-ICR MS) routinely achieves the ultrahigh mass resolving power sufficient to separate and accurately assign elemental compositions to ionized components of highly complex mixtures.[64−68] This includes SOM and dissolved organic matter (DOM),[69−86] solid and water-soluble char residues,[61,87−94] and petroleum,[95−100] where the m/z differences can be as small as the mass of an electron.[101] The characterization of both field-[61,87] and laboratory[87,89]-produced char have provided insight into molecular-level changes to different organic matter substrates induced by heating; however, limited information connects compositional changes in charring SOM to changes throughout progressive fire intensity gradients and the enhanced mobility of water-soluble organic nitrogen following a fire.

The soil samples selected for this study originate from Boulder County, CO, USA, to simulate SOM from forested watersheds, similar to those affected by the High Park fire in 2012 and Cameron Peak fire in 2020 (northern Colorado).[102] While DOM does exhibit unique characteristics that can be used to distinguish different sources,[83] many of its features are remarkably consistent.[103] Dissolved pyrogenic organic matter also has common characteristics that can be observed at numerous sites and locations.[40,88,104] Therefore, these samples were considered representative of soil from similar sites in the western United States and Canada, where forest fires and their effects on ecosystems and watersheds currently generate tremendous interest and concern. Organic carbon quantification[105,106] and solid-state ^{13}C NMR[106] have been previously reported for these samples. Additionally, benzene polycarboxylic acids (BPCAs) and pyridinic analogues were identified by quadrupole time-of-flight mass spectrometry as biomass burning markers (>150 °C).[106] These findings only address a fraction of the molecules present during heating, suggesting that ultrahigh-resolution mass spectrometry is required to develop a more complete picture of the compositional changes that occur during heating.

Here, we present a compositional comparison of water-extractable, acidic SOM species produced at discrete temperatures (i.e., 150, 250, 350, and 450 °C) by negative ESI FT-ICR MS. This study focuses on nitrogen-containing residues due to their enrichment during the previous analysis[105] of the samples studied here and importance in ecosystem recovery following fires. We compare and catalog molecular transformations of nitrogen species in heated SOM at discrete temperatures by FT-ICR MS. Mass difference-based analysis is performed to identify potential reaction products formed during heating and suggest potential pathways in heated SOM as a function of temperature.

MATERIALS AND METHODS

Site Description and Sample Processing. Soil samples were collected from the south of the Gross Reservoir in Boulder County at 2222 m above the sea level during the summer of 2016 and correspond to site H samples in the reports of Thurman et al.[106] In brief, triplicate soil samples were collected within 10 m of each other in 1 m^2 transects with a shovel at a depth of 1−5 cm after visible litter and vegetation debris were removed. The surrounding overhead vegetation was composed of four main coniferous tree species varying in density: ponderosa pine (*Pinus ponderosa*), lodgepole pine (*Pinus contorta*), limber pine (*Pinus flexilis*), and Douglas fir (*Pseudotsuga menziesii*). Understory vegetation for the sampling area included a mix of grasses, forbs, and shrubs, largely dominated by cheatgrass (*Bromus* spp.) and Canada thistle (*Cirsium arvense*). Following sampling, the soils were distributed on metal trays 1 cm deep and oven-dried at 100 °C for 2 h to eliminate moisture and to suppress the survival of microbial communities present in the soil[107] that may compromise sample integrity during storage. The soil was passed through a 2 mm (no. 10) stainless-steel sieve to remove large rocks and through a 0.841 mm (no. 20) sieve to remove smaller plant matter before storage.

Simulated Laboratory Heating and Leachate Preparation. Soils were heated in an electric muffle furnace at the temperatures of 150, 250, 350, and 450 °C in 90 mL porcelain dish crucibles using a Lindberg/Blue Box Furnace model BF51442C with a Lindberg Furnace Power Supply Controller model 59344. To ensure uniformity in soil heating, each soil sample was separated into 10 g per crucible (approximately 0.5 cm high) and heated in batches of 10 crucibles for a total of 100 g of the soil sample at each temperature. Batches were held at each temperature under atmospheric conditions for 2 h, cooled to room temperature, and then stored in 40 mL amber glass vials at −5 °C until used. The furnaced samples were then leached for 24 h in deionized water at 5 g of soil per liter. The leachates were decanted and filtered using a 0.45 μm glass fiber syringe filter. A portion of the leachates were freeze-dried and used in organic carbon and nitrogen analysis on the solid soil and leachates and have been described elsewhere.[106] Section

https://doi.org/10.1021/acs.est.1c06745
Environ. Sci. Technol. 2022, 56, 4597−4609

S2 in the Supporting Information contains additional information on this method to simulate the effects of a wildfire.

The aqueous leachates were fractionated using hydrophobic and hydrophilic resins, as previously described.[106] In brief, aqueous leachates were fractionated into hydrophobic (XAD-8) and hydrophilic (XAD-4) fractions to facilitate better separation and identification of SOM features and their properties.[27,64] Section S3 in the Supporting Information provides a full description of the fractionation procedure.

Fourier Transform Ion Cyclotron Resonance Mass Spectrometry. Resin extracts were resolubilized in methanol (HPLC grade, Sigma-Aldrich Chemical Co., St. Louis, MO) at 50 ppm carbon concentrations prior to analysis. Each sample solution was infused via a microelectrospray ionization (ESI) source operated in the negative mode.[108] DOM extracts were analyzed with a custom-built 9.4 T FT-ICR mass spectrometer and absorption mode mass spectra calibrated and assigned as previously described.[109,110] Section S4 of the Supporting Information provides a full description of the FT-ICR MS operating conditions and data processing procedure. Formulas containing carbon (C), hydrogen (H), oxygen (O), nitrogen (N), and sulfur (S) were assigned using the experimentally measured masses and converted from the International Union of Pure and Applied Chemistry mass scale to the Kendrick mass scale[111] for the rapid identification of homologous series for each heteroatom class (i.e., KMD_{CH_2} for species differing only by degree of alkylation)[112] using PetroOrg software.[64,113−115] Molecular formula assignments with an error >0.5 ppm were discarded, and only heteroatom ($N_xO_yS_z$) classes with a combined relative abundance of ≥0.15% of the total were considered. Formulas were used to calculate ring-plus-double-bond (to carbon) equivalents (RDBE = $1 + c - h/2 + n/2$),[114,115] where c, h, n, o, and s refer to the stoichiometric carbon, hydrogen, oxygen, nitrogen, and sulfur, respectively. Formulas were also used to calculate modified aromaticity indices (AI_{Mod}),[116,117] which estimate the density of unsaturated carbon after assuming that a portion of the RDBE is not attributable to carbon−carbon bonds (e.g., carbonyl or carboxyl functional groups).

RESULTS AND DISCUSSION

Bulk Heating Effects on Organic Carbon and Nitrogen. The organic carbon and nitrogen content has been previously reported for these samples[105,106] and will be used here to support compositional analysis by FT-ICR MS. Table S1 shows the total organic carbon (TOC), total organic nitrogen (TON), water-extractable organic carbon (WEOC), and water-extractable organic nitrogen (WEON), and also inorganic nitrogen measurements (NO_2−N, NO_3−N, and NH_4−N). In brief, the TOC and TON decreased continuously from the control (46.303 ± 0.000 mg TOC/g soil, 2.179 ± 0.004 mg TON/g soil) to 450 °C (1.435 ± 0.001 mg TOC/g soil, 0.315 ± 0.000 mg TON/g soil) with increased rates of removal at temperatures >150 °C. The WEOC and WEON changed from the control (0.485 ± 0.004 mg WEOC/g soil, 0.032 ± 0.004 mg WEON/g soil) during heating, reaching a maximum at 250 °C (2.247 ± 0.036 mg WEOC/g soil, 0.211 ± 0.002 mg WEON/g soil) and minimum at 450 °C (0.065 ± 0.002 mg WEOC/g soil, 0.008 ± 0.002 mg WEON/g soil). The difference in magnitude of the water-extractable fraction and total SOM content suggests that most of the SOM was mineralized during heating and thus did not partition into water at any temperature.

Table S2 shows the C/N ratios of the total (TOC/TON) and water-extractable (WEOC/WEON) fractions. Both decrease from the control (total: 21.24, water-extractable: 15.16) to 250 °C (total: 14.77, water-extractable: 10.63) and further by 450 °C (total: 4.56, water-extractable: 8.10). Nitrogen is enriched in both the solid and water-extractable fractions at temperatures ≥250 °C. Additionally, the WEOC/WEON does not lower to the same extent as the TOC/TON at 350 and 450 °C, which may indicate that a larger proportion of carbonaceous residues are mineralized directly from the solid phase, as opposed to undergoing a reaction that would increase water solubility.

Solid-State ^{13}C NMR Spectroscopy. Solid-state CP/MAS and DP/MAS ^{13}C NMR spectra of the hydrophobic acid (XAD-8) and hydrophilic acid (XAD-4) samples were described in detail previously.[106] The CP/MAS spectra are reproduced in Figures S1 and S2 and the integrations in Table S3. In brief, the spectrum of the hydrophobic acid sample at 150 °C shows a relative increase in the proportion of the C-alkyl carbon peak (0−60 ppm) above the control. From 150 to 450 °C, there are successive decreases in the C-alkyl carbon, O-alkyl carbon (60−90 ppm), aromatic/acetal carbon (90−110 ppm), and ketone/quinone carbon (190−230 ppm) peaks and a narrowing of the aromatic carbon (110−190 ppm) and carboxyl/amide (160−190 ppm) carbon peaks. Peptide amides are assumed to have been destroyed by 350 °C. The residual aromatic carbon peaks at 131 ppm and carboxylic acid peaks at 172 ppm in the 350 and 450 °C spectra are consistent with the benzene and pyridine carboxylic acids as previously reported[106] among other constituents. The spectra of the hydrophilic acid samples follow a similar pattern from control to 350 °C, with the exception that the latter spectrum shows residual C-alkyl and O-alkyl carbon peaks at 30 and 65 ppm, respectively. Comparison of the control hydrophobic and hydrophilic acid spectra shows that water-extractable soil carbohydrates preferentially isolate on the XAD-4 resin, indicated by the carbohydrate peaks at 72 and 102 ppm in the hydrophilic acid spectrum. These peaks are significantly reduced in the hydrophilic acid spectra from the 250 and 350 °C samples, confirming destruction of the carbohydrate material in the soil at these temperatures.

The quantities of hydrophobic and hydrophilic acid samples isolated (∼10−90 mg) were insufficient for the analysis of naturally abundant nitrogen by solid-state ^{15}N CP/MAS NMR, within reasonable spectrometer accumulation times. However, losses or transformation of nitrogen functionalities with temperature can be inferred from the ^{13}C NMR spectra and are listed in Table S4. The forms of nitrogen in SOM, not impacted by fire or heat, may include amines (terminal amino groups of amino acids, amino sugars, primary amines of purine and pyrimidine bases, and primary and secondary amino-quinones), peptides, N-acetylated sugars, the imide and lactam nitrogens of nucleotide bases, and heterocyclic nitrogens such as pyrrole, indole, and imidazole. Carbons alpha to the amine group of amino acids in peptides have ^{13}C chemical shifts in the range from 40 to 65 ppm, while ring carbons bonded to the amine group in amino sugars have chemical shifts in the approximate range from 50 to 60 ppm. These are in the range of sp^3-hybridized carbons that decrease in the ^{13}C NMR spectra of the hydrophobic acid (XAD-8) fractions from 150 to 250 °C and have disappeared from 350 to 450 °C (Figures S1

https://doi.org/10.1021/acs.est.1c06745
Environ. Sci. Technol. 2022, 56, 4597−4609

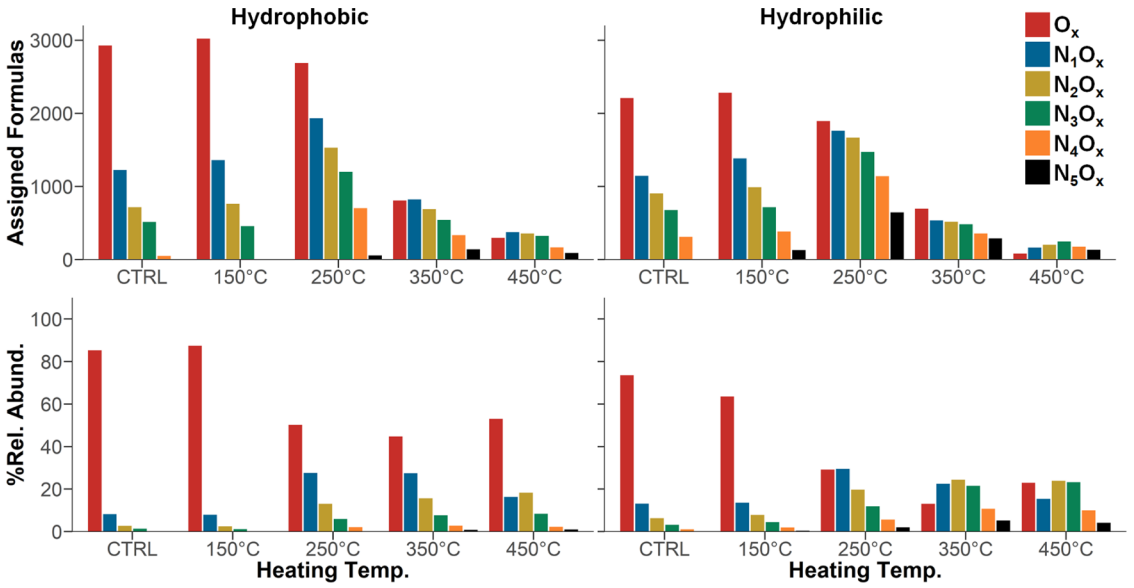

Figure 1. Number of assigned molecular formulas (top) and percent relative abundance (bottom) of the CHO and CHNO heteroatom classes at each temperature measured by the 9.4 T FT-ICR MS using negative ESI. CHNO classes are distinguished by the nitrogen content ($N_{1-5}O_x$).

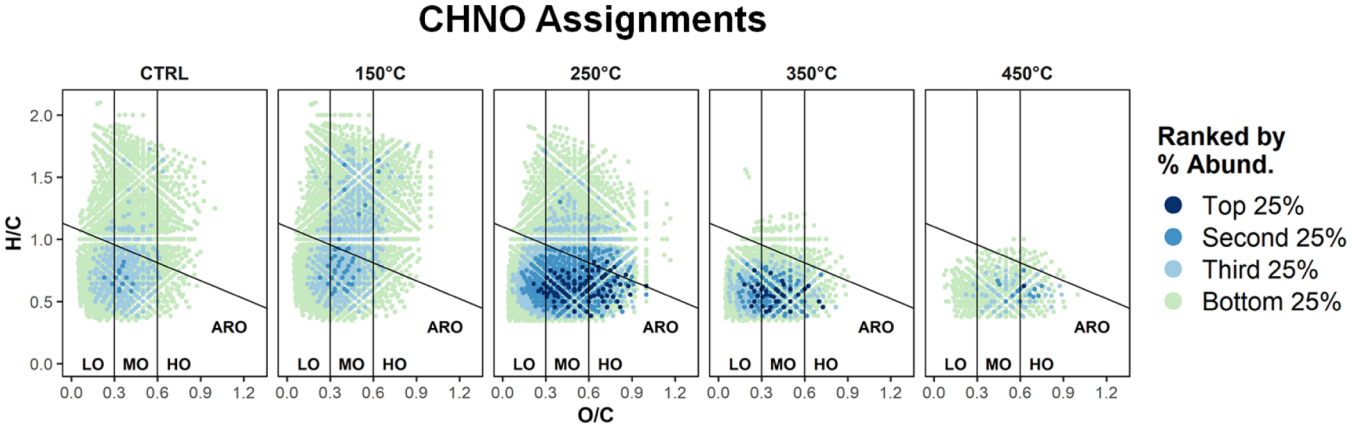

Figure 2. Abundance-weighted VK plots of the N_xO_x species derived from negative-ion ESI FT-ICR MS spectra for the unburnt control (CTRL) and heated soil leachates isolated on the hydrophilic resin. Lines were added to each plot to indicate regions where aromatic features predominate ($AI_{Mod} \geq 0.5$, indicated by the ARO line), and relative oxygen density: "LO" = low oxygen density, $O/C \leq 0.3$; "MO" = mid-oxygen density, $0.3 < O/C \leq 0.6$; "HO" = high oxygen density, $O/C > 0.6$. The plotted formulas were grouped using their abundances, where the "top 25%" (dark-blue points) are 25% of the sample's cumulative abundance comprising the most abundant formulas, the "second 25%" are the next 25% comprising the next most abundant formulas, and so on.

and S2). Therefore, removal or transformation of amino acid, peptide, and amino sugar structures in the soil to leachable aromatic nitrogen compounds or volatile degradation products, including nitrogen gases, is a reasonable inference from these ^{13}C NMR spectra. Nitrogen-containing functionalities encompassed within the 100−190 ppm chemical shift region of the residual peaks between the 350 and 450 °C spectra would be limited to nonpeptide amide and aromatic heterocyclic structures. Of the water-extractable organic matter (WEOM) that sorbs to the XAD-4 resin, the ^{13}C NMR spectra also indicate a decrease, but not total destruction, of amino acid, peptide, and amino sugar structures from 150 to 350 °C (Figure S2).

WEOM: Proliferation of Nitrogen-Containing Heteroatom Classes. Broadband negative ion ESI FT-ICR mass spectra for hydrophobic and hydrophilic fractions as a function of temperature are shown in Figures S3 and S4, respectively. All samples spanned a similar molecular weight range between m/z 150−600 with an achieved resolving power >1,500,000 at m/z 400. Figure 1 shows the number of assigned formula and percent relative abundance of the CHO (O_x) and CHNO heteroatom classes separated by the nitrogen content ($N_{1-5}O_x$). Counts for each class can be found in Table S5, alongside the abundance-weighted average C/N ratios and m/z, discussed below. The CHO and CHNO assigned molecular formulae from the control (hydrophilic: 5518 and hydrophobic: 5846) increased slightly at 150 °C (hydrophilic: 6149 and hydrophobic: 5960) and the most at 250 °C (hydrophilic: 8770 and hydrophobic: 8554). Assignments decreased at 350 °C (hydrophilic: 2948 and hydrophobic: 3584) and reached a minimum at 450 °C (hydrophilic: 1035, hydrophobic: 1734).

Importantly, only the CHNO assignments contributed to the increased formulae at 250 °C and remained the largest class, containing over 70% of the formulas assigned at intensities ≥250 °C in both fractions (Figure 1, top). The percent relative abundance of the heteroatom classes followed

https://doi.org/10.1021/acs.est.1c06745
Environ. Sci. Technol. 2022, 56, 4597−4609

Figure 3. Percent relative abundance of CHNO classes in the unburnt (CTRL) and heated (150−450 °C) hydrophilic samples separated by the nitrogen and oxygen ($N_{1-4}O_{2-15}$) content. The N_5O_{2-15} and assignments from the hydrophobic fraction can be found in Figures S8 and S9, respectively.

a similar trend: class abundances changed slightly below 250 °C, after which the CHNO classes in the hydrophilic fraction increased to ∼75% and the hydrophobic fraction up to ∼50% of the total abundance at temperatures ≥250 °C (Figure 1, bottom). Of the CHNO assignments, the $N_{2\text{-}5}O_x$ classes appeared to increase the most in assignments at 250 °C. At higher temperatures, the $N_{2\text{-}5}O_x$ assignments generally decreased less than the N_1O_x assignments. The increase in relative abundances for $N_{2-5}O_x$ is also reflected by the average weighted C/N ratio (Table S5) that decreased from 250 to 450 °C (hydrophilic: 9.61 to 5.46 and hydrophobic: 12.31 to 8.03).

Despite a similar trend between fractions of increased CHNO assignments and abundance above 150 °C, in the hydrophobic fraction, the CHO class retained ∼50% of the relative abundance at 350 and 450 °C but was composed of fewer, highly abundant peaks. These assignments included BPCAs that were previously measured in these samples from 250 to 450 °C and were found to be concentrated in the hydrophobic fraction.[106] Other CHO assignments that are only abundant in the hydrophobic fraction at 350 and 450 °C also appeared to be related by carboxylic acid groups, some matching formulas tentatively identified by Ferrer et al.[118] Pyridinic analogues to BPCAs were also tentatively identified at low concentration in the hydrophilic fraction only[106] but only corresponded to two assignments in the current study. Interestingly, numerous other CHNO assignments were assigned at higher abundance throughout the temperature gradient in the hydrophilic fraction and to a lesser extent in the hydrophobic fraction. These are explored below.

Speciation of the Water-Extractable Nitrogen-Containing Residues. The hydrophilic fraction was the focus throughout the rest of this study based on the increase in WEON and corresponding increase in CHNO formula assignments that appeared better isolated in the hydrophilic fraction. While generally similar, differences will be noted for the hydrophobic fraction and analogous figures can be found in the Supporting Information.

Figure 2 displays the van Krevelen (VK) plots of the CHNO assignments, which can be used to infer changes to saturation and oxygen content throughout the temperature gradient in the hydrophilic fraction (Figure S5 for the hydrophobic fraction). Unique and common assignments between fractions are illustrated in Figure S6. In the control (CTRL), the CHNO assignments before heating (bottom, third, and second 25% bins) displayed coverage over a large range of H/C (∼0.4. to 2.0) and O/C (∼0.1 to 1.0) values, typical of a heterogeneous WEOM mixture.[27,77,119,120] At 150 °C, peaks encompass similar regions to the CTRL and also include additional assignments at H/C > 1, above the ARO line. These midsaturated and aliphatic CHNO species at 150 °C may result from the release of plant, root, and microbial residues that can occur at this temperature.[17,121] At 250 °C, CHNO assignments in the aromatic plot region (below the ARO line) increased in abundance and midsaturated and aliphatic features decreased.

The enriched aromatic regions were more pronounced at 350 and 450 °C, with high abundance peaks encompassing a narrower range and fewer assignments. The changes in saturation are also reflected by the RDBE, which is visualized in Figure S7 by the nitrogen content ($N_{1-5}O_x$). While the hydrophilic and hydrophobic fractions were generally similar, high RDBE peaks (relative to the control) at 350 and 450 °C were only attributed to $N_{2-5}O_x$ formulas in the hydrophilic fraction. The nitrogen dense assignments exhibited increased abundance and aromaticity during heating, which is in good agreement with the ^{13}C NMR.

The most abundant O/C regions also appeared to shift during heating. At 250 °C, aromatic plot regions were enriched across all O/C but enriched most in mid- and high-oxygen aromatic plot regions. The most abundant aromatic plot region shifted at 350 °C to lower O/C, encompassing the low- and mid-oxygen density regions. Finally, at 450 °C, abundant peaks

https://doi.org/10.1021/acs.est.1c06745
Environ. Sci. Technol. 2022, 56, 4597−4609

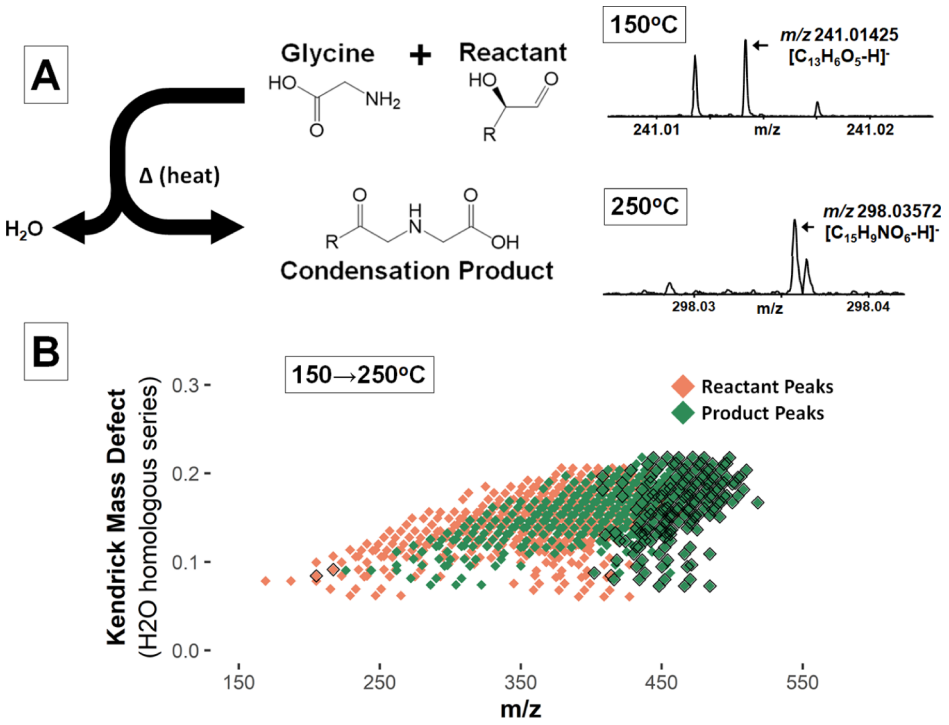

Figure 4. Scheme and visualization of the Maillard reactant−product pairs that were identified throughout the temperature transitions that correspond with a Gly condensation. (A) Simplified scheme of a glycine condensation reaction using a generic reactant and product, where the exact mass difference is 57.02146 Da. Single peaks are shown and labeled that match a Gly condensation mass difference across the 150 → 250 °C transition and are present in a KMD_{H_2O} series of ≥3 peaks and (B) plot of the KMD_{H_2O} series matching the Gly condensation in the 150−250 °C transition. Data was truncated for ease of visualization. Reactants (orange) and products (green) were outlined if they were unique to 150 or 250 °C, respectively.

were in high-oxygen density regions and in mid-oxygen regions to a lesser extent, although fewer peaks were present to indicate a trend.

To explore the shift in oxygen content further, Figure 3 displays the percent relative abundance of the CHNO classes separated by nitrogen and oxygen ($N_{1-4}O_{2-15}$) (hydrophilic N_5O_{2-15} and hydrophobic fraction in Figures S8 and S9, respectively). Features were similar between the control and 150 °C sample, where nitrogen classes were centered around $N_{1-4}O_{5-6}$ or were too low in abundance to detect (i.e., N_5O_x). At 250 °C, the N heteroatom classes increased both in abundance and oxygen number, and several new CHNO classes (N_1O_{13-15}, $N_{2-4}O_{11-14}$, and N_5O_{3-10}) were assigned. This could indicate multiple oxidation reactions by N- and O-containing species or condensation reactions among SOM species.

At 350 °C, the abundances of N_xO_{10-15} species decreased greatly or disappeared entirely, and the oxygen numbers of the most abundant N heteroatom classes decreased, now centering around N_1O_{4-5} and $N_{2-5}O_4$. The abundance-weighted average m/z and C/N of the detected peaks also changed more between 250 and 350 °C than at any other temperature transition, decreasing from 315.15 to 266.11 m/z and 9.61 to 7.01 C/N (Table S5). This could indicate the loss of O-containing species through dehydration, decarboxylation, or other fragmentation reactions. At 450 °C, the most abundant heteroatom classes rose in oxygen number from 350 °C; however, each of the class distributions became less uniform. Specific classes appeared enriched at 450 °C (e.g., N_2O_6 and N_2O_8), potentially corresponding to specific char products.

While the most abundant N_xO_x class at each temperature differed depending on the amount of nitrogen assigned, the increase and decrease in the oxygen content between 150 and 350 °C appeared to occur consistently across every nitrogen class. The trend observed here might suggest the presence of distinct transformations and features in each of the classes, dependent on temperature. In such complex samples, it is difficult to discern whether nitrogen-containing species are persistent once formed, formed continuously as new by-products through heating, or a combination of both. Similarly, it is difficult to determine if decreasing or disappearing peaks are attributable to new or enriched peaks upon heating or mineralization. Nevertheless, formation mechanisms that contribute to the observable nitrogen enrichment can be studied if known transformations throughout the temperature gradient can be modeled.

Modeling Maillard Reaction Processes. The Maillard reaction involves the condensation of reducing sugars with amino acids, followed by many more reactions, and is well known in the context of cooking and preparing food.[57] In fact, many Maillard reaction intermediates and fragments, referred to here as Maillard Reaction Products (MRPs), have been well described and characterized in food chemistry using simple systems.[122−125] Hemmler et al.[126] studied MRPs by heating equimolar mixtures of ribose and glycine at 100 °C for up to 10 h. They reported several findings consistent with the behavior of WEOM in this study, including the enrichment of aromatic nitrogen and increased N_2O_x assignments following heating longer than 4 h and the presence of several reaction pathways that dominated the MRPs within 6 h. These factors

https://doi.org/10.1021/acs.est.1c06745
Environ. Sci. Technol. 2022, 56, 4597−4609

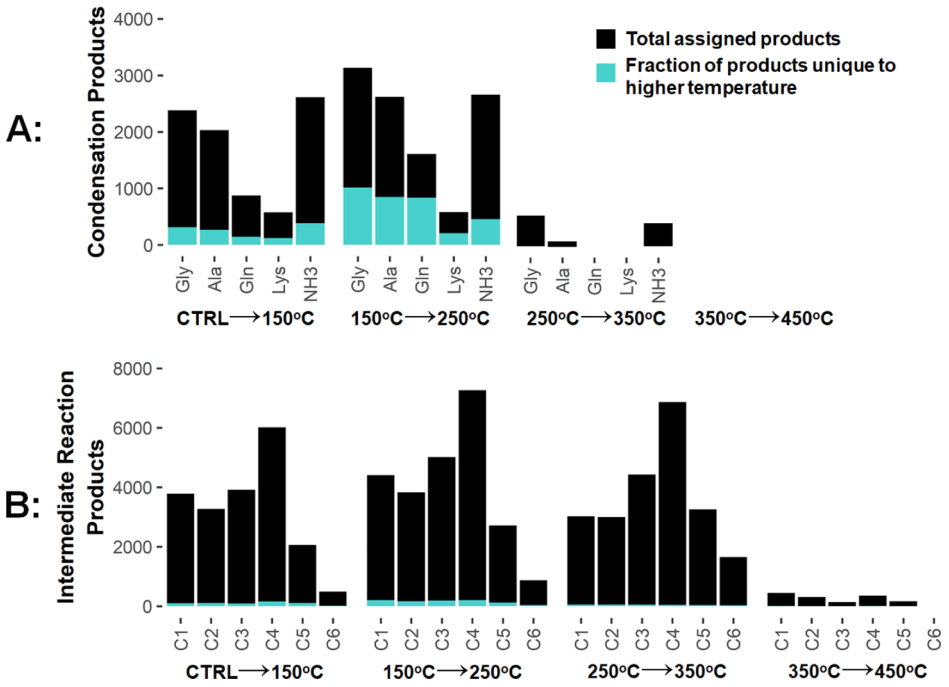

Figure 5. Number of product assignment matching reactions with predicted mass differences along the Maillard reaction pathway at each temperature transition from the hydrophilic sample fractions. Blue bars within each plot indicate the number of products that were newly assigned at the higher temperature only. (A) Counts for product peaks matching amino acid condensations or ammonia additions. (B) Intermediate reaction products were separated by the carbon number (C#) of the fragment lost, ranging from C1 (e.g., formic acid) to C6 (e.g., glucosone). For a complete list of all the amino acid condensation and C# fragment compositions, see Table S6.

motivated the exploration of Maillard reaction pathways in the current study.

Potential MRPs were identified using a mass difference-based analysis that is depicted in Figure 4. Mass differences were computed between peaks based on known Maillard reactions, where potential Maillard "precursor" and "product" peaks were identified going from lower to higher temperatures, respectively, when they differed by the expected mass difference, using the theoretical masses of the assigned formulas (Table S6). For instance, a peak at 150 °C needed to differ from a peak at 250 °C by the exact mass of the reaction of interest to be considered a potential MRP. In a complex biogeochemical mixture such as SOM, it is possible that some of the expected mass differences will occur by chance or due to the presence of common structures in SOM molecules. For this reason, the best evidence of potential MRPs comes from (i) product peaks that were not detected at the lower temperature or (ii) product peaks that were present at both temperatures but whose abundances increased relative to the corresponding precursor peaks at the higher temperature.

The temperature transitions studied here were CTRL → 150 °C, 150 → 250 °C, 250 → 350 °C, and 350 → 450 °C. The reactions modeled included amino acid condensations, where glycine (Gly), alanine (Ala), glutamine (Gln), and lysine (Lys) were chosen based on their presence in soil[127] and the contributions of peptidoglycan and other microbial biomass to SOM.[128−131] Hemmler et al.[126] reported that the initial condensation reaction was followed by an extended series of dehydration reactions, leading to MRPs with greater degrees of unsaturation and aromaticity, so tentative MRPs were only considered when they occurred in "dehydration series" associated with successive water losses ($n \geq 3$). These were identified in these samples using a modified Kendrick mass defect analysis (KMD_{H_2O}) based on the accurate mass of water (IUPAC mass × 18/18.01057)[123,126,132] and can be visualized in Figure S10, which plots a subset of dehydration series for N_3O_x assignments.

Ammonia (NH_3) addition was studied as an alternative pathway for nitrogen enrichment because ammonia was retained here (Table S1) and is retained in soil after fires,[133,134] and fire-derived organic matter has been reported to retain ammonia through covalent bond formation.[133] Peaks were also examined for the loss of byproducts specific to the Maillard reaction pathway (Table S6), which are referred to here as intermediate reaction products. The intermediate reaction products are identified by the size of the carbon fragment (C#) lost, ranging from C1 (e.g., formic acid) to C6 (e.g., glucosone).[123,126,135] These C# include carbonyl-containing species (e.g., α-hydroketones and α-hydroxyaldehydes) that can react further to form heterocyclic nitrogen.[135] The reactions studied here were not intended to include every possible reaction but to investigate whether some of the changes in WEOM composition during soil burning could be modeled with time-resolved Maillard reactions previously observed in simpler systems.

Molecular Evidence of Maillard Reactions and Ammonia Additions. Figure 4 displays the product counts for each of the potential condensation and intermediate reaction pairs. Condensation products and ammonia additions were observed in the CTRL → 150 °C (8473 total), 150 → 250 °C (10 595 total), and 250 → 350 °C (3363 total) temperature transitions (Figure 4A). Intermediate reaction products were also found at each of the transitions and were also highest in the 150 → 250 °C transition (24 081 total) (Figure 5B). The hydrophobic fraction exhibited similar trends

https://doi.org/10.1021/acs.est.1c06745
Environ. Sci. Technol. 2022, 56, 4597−4609

but at lower counts and can be seen in Figure S11. It is worth noting that in the hydrophilic fraction, the average m/z of the assigned formulae increased the most at 250 °C and decreased the most at 350 °C (Table S5).

The condensation and ammonia addition reaction pairs shared some of the same product peaks and are shown numerically in Venn diagrams in Figure S12. This is most prominently observed in the 150 → 250 °C transition with the Gly and Ala condensation reactions that shared 2065 of their total product peaks (Gly: 3132 and Ala: 2619) with each other and ammonia addition pairs. This could indicate that different reactions create product peaks with identical elemental compositions, which is certainly possible in such a complex mixture, but it also highlights the difficulty of evidencing specific reactions in a complex mixture. Importantly, the condensation product peaks also included assignments that were unique to the higher temperature and to only one modeled reaction (Figures 5 and S11). These product peaks present the clearest evidence of specific Maillard reactions in the burned soil systems. They are not dispositive, but they are numerous and consistent with previous observations from much simpler systems.[126] These findings are also supported when considering the loss of carbohydrate signatures by 350 °C in the ^{13}C NMR that coincided with the decrease in assigned MRPs. Similarly, the evidence of unique ammonia additions is not dispositive, but they are numerous and their occurrence is consistent with previous reports.[133]

In comparison, many of the intermediate reaction products were common to at least one of the other C# reaction pairs or peaks assigned at lower temperatures and are shown numerically in Venn diagrams in Figure S12. It seems likely that the high relatedness between the intermediate reaction products and assignments at lower temperatures is due to SOM complexity and the multitude of pathways occurring to individual compounds during heating. Studies[126,136] have reported an exponential increase in MRPs when nitrogen was present during the heating of simple systems, so it seems reasonable that numerous transformations can occur for a single residue. Still, the presence of intermediate reaction products from 250 → 350 °C and the absence of condensation products does correspond to the decreased N_xO_{10-15} and increased N_xO_{3-6} class abundances and lower average m/z.

The presence of shared and uniquely assigned product peaks suggests that products appear to be forming as a function of specific amino acid reactions and also inorganic nitrogen additions. It should be noted that in a study measuring ribose-amino acid products formed during heating at 100 °C, Hemmler et al.[136] indicated that reactions with Lys produced the most products and had the highest reactivity, and Gly had the lowest, up to N_4O_x. In our study, the order was Gly (3132) > Ala (2619) > Gln (1606) > Lys (580). The discrepancy might originate from differences in source materials and the higher temperatures used, or it might result from confounding mass differences in such a complex material. Ammonia appeared to contribute to the products through inorganic nitrogen addition, but other pathways such as nitration may also be valid for inorganic nitrogen enrichment of WEOM. Finally, reactions between the MRPs formed may contribute to the relative increase of $N_{3-5}O_x$ classes in SOM at above 250 °C, but the investigation of these reactions or persistent products would require a more precise understanding of the specific MRPs formed during heating.

Environmental Implications. While the experimental design of this study was a proxy for soil heating in the field, the temperatures used here are reflective of temperatures in the organic soil horizon in mineral soils during wildfires. Low-severity heating (e.g., fast-moving, prescribed fires) can produce temperatures as low as 50 °C at 5 cm depths, and high-severity heating (e.g., slow-moving, smoldering fires) can reach temperatures of >250 °C at up to 10 cm depths with potential to last from minutes to several days.[26] Patterns in the molecular formulae identified here were not observed up to 450 °C, which corresponds to the near total consumption of SOM and WEOM at 450 °C in this study and elsewhere.[26,38] Most residues were removed completely when heating to this temperature; therefore, residues from 150 to 350 °C will predominate when studying fire-affected field sites, despite the heterogeneity in wildfire intensities. This implies that SOM at specific soil depths within this temperature range will be responsible for what is being leached from soils.

The apparent solubility of the charred organic matter is somewhat contrary to the formation of hydrophobic features[104] and has numerous implications for postfire watershed and water quality conditions. The mobility of these residues not only removes an organic carbon and nitrogen source at the site of the burn, but the absence of plants and plant nutrient uptake following fires will increase the subsurface transport of the WEOM.[137] This removal is associated with an initial pulse of nutrients during the fire and long-term leaching that will influence stream biota metabolism[138,139] and could correspond to the changes in the microbial community structure observed following fires with implications regarding C storage in fire-affected ecosystems.[140] Interestingly, the enriched aromatic CHNO observed here is not considered a reactive precursor for DBP formation during water treatment.[141−143] It is possible that the CHNO fractions containing alkylated amine precursors are not well represented in the samples studied here as the ionization mode used for mass spectrometry was not amenable to basic nitrogen moieties;[144,145] however, these groups are often transformed during even moderate heating.[146]

This study employed a laboratory-based heating method to exert the most control over the experimental conditions. The general trend in aromaticity was consistent with other laboratory-[87] and field-based[61,88] SOM chars analyzed by FT-ICR MS. The enriched nitrogen observed here is also common to chars with proteinaceous biomass, such as grasses.[42,89,93,147] While the results of this study focus on a laboratory-simulated microcosm that represents transformations that occur with heating in the field, the observed changes in aromaticity, changes in nitrogen density relative to the oxygen content, and mass-difference analysis provide evidence for SOM-specific transformations such as Maillard reactions that have been reported in simpler systems. The occurrence of MRPs here is not the definitive evidence of Maillard reactions due to the qualitative analysis by FT-ICR MS but does support the existence of Maillard reactions when considering the existing knowledge of Maillard reactions,[36,60,126,136] the well-known presence of amino acid and carbohydrate functionalities in SOM,[127−131] and the observed enrichment of N-containing compounds in SOM during heating here and elsewhere.[42,55,58,59]

Without knowledge of the precise precursors present in the SOM, a comprehensive understanding of how the Maillard reaction applies to transformations in heated SOM remains

https://doi.org/10.1021/acs.est.1c06745
Environ. Sci. Technol. 2022, 56, 4597−4609

uncertain. However, the evidence presented here suggests that the Maillard reaction pathway can in part describe transformations in heated SOM. Interestingly, the potential MRPs and their reactions appeared to be specific to heat intensity, such that the trends and unique peaks might contribute new N-containing biomass burning markers specific to fire intensity. The introduction of known precursor materials, such as specific amino acids, to SOM during controlled heating could more clearly identify product residues that are associated with Maillard reaction pathways.

■ ASSOCIATED CONTENT

Supporting Information

The Supporting Information is available free of charge at https://pubs.acs.org/doi/10.1021/acs.est.1c06745.

Measured quantities of carbon and nitrogen; ^{13}C NMR, FT-ICR MS spectra, and analogous figures of the hydrophobic fraction presented here; explanation for the use of muffle furnaces for the soil heating experiments; description of the resin-based fractionation; and description of the FT-ICR MS settings and protocol (PDF)

■ AUTHOR INFORMATION

Corresponding Author

Thomas Borch − *Department of Chemistry, Colorado State University, Fort Collins, Colorado 80523-1872, United States; Department of Soil and Crop Sciences, Colorado State University, Fort Collins, Colorado 80523-1170, United States;* orcid.org/0000-0002-4251-1613; Phone: +1 (970)491-6235; Email: thomas.borch@colostate.edu

Authors

William Bahureksa − *Department of Chemistry, Colorado State University, Fort Collins, Colorado 80523-1872, United States;* orcid.org/0000-0003-3056-3595

Robert B. Young − *Department of Soil and Crop Sciences, Colorado State University, Fort Collins, Colorado 80523-1170, United States;* Present Address: Chemical Analysis and Instrumentation Laboratory, New Mexico State University, Las Cruces, NM 88003−8006, United States; orcid.org/0000-0001-7485-0604

Amy M. McKenna − *Department of Soil and Crop Sciences, Colorado State University, Fort Collins, Colorado 80523-1170, United States; National High Magnetic Field Laboratory, Florida State University, Tallahassee, Florida 32310-4005, United States;* orcid.org/0000-0001-7213-521X

Huan Chen − *National High Magnetic Field Laboratory, Florida State University, Tallahassee, Florida 32310-4005, United States;* orcid.org/0000-0002-6032-6569

Kevin A. Thorn − *U.S. Geological Survey, Earth System Processes Division, Water Mission Area, Lakewood, Colorado 80225-0001, United States*

Fernando L. Rosario-Ortiz − *Department of Civil, Environmental, and Architectural Engineering, University of Colorado, Boulder, Colorado 80309-0607, United States; Environmental Engineering Program, University of Colorado, Boulder, Colorado 80309-0428, United States;* orcid.org/0000-0002-3311-9089

Complete contact information is available at: https://pubs.acs.org/10.1021/acs.est.1c06745

Author Contributions

The manuscript was written through contributions of all authors. All authors have given approval to the final version of the manuscript.

Notes

The authors declare no competing financial interest.

■ ACKNOWLEDGMENTS

This research was funded by the National Science Foundation (1512670 and 2114868) and the USDA National Institute of Food Agriculture through AFRI grant no. 2021-67019-34608. A portion of this work was funded by the National Science Foundation Division of Chemistry and Division of Materials Research through NSF DMR-1644779 and the state of Florida. We specifically thank Ariel Retuta, Yun Yu, and Heena Duggal for their contributions regarding sample preparation and data analysis. We are also thankful to Michael J. Wilkins (CSU) and Charles C. Rhoades (USDA FS) for their review comments and help with this project. Any use of trade, firm, or product names is for descriptive purposes only and does not imply endorsement by the U.S. Government.

■ REFERENCES

(1) NIFC. *National Large Incident Year-to-Date Report*, 2020.

(2) Hoover, K.; Hanson, L. A. Wildfire Statistics. *Congressional Research Service*, 2021, 2.

(3) Nolan, R. H.; Boer, M. M.; Collins, L.; Resco de Dios, V.; Clarke, H.; Jenkins, M.; Kenny, B.; Bradstock, R. A. Causes and consequences of eastern Australia's 2019-20 season of mega-fires. *Glob. Chang. Biol.* **2020**, *26*, 1039−1041.

(4) Walker, X. J.; Baltzer, J. L.; Cumming, S. G.; Day, N. J.; Ebert, C.; Goetz, S.; Johnstone, J. F.; Potter, S.; Rogers, B. M.; Schuur, E. A. G.; Turetsky, M. R.; Mack, M. C. Increasing Wildfires Threaten Historic Carbon Sink of Boreal Forest Soils. *Nature* **2019**, *572*, 520−523.

(5) Martin, D. A. At the Nexus of Fire, Water and Society. *Philos. Trans. R. Soc., B* **2016**, *371*, 20150172.

(6) Ruffault, J.; Curt, T.; Moron, V.; Trigo, R. M.; Mouillot, F.; Koutsias, N.; Pimont, F.; Martin-StPaul, N.; Barbero, R.; Dupuy, J.-L.; Russo, A.; Belhadj-Khedher, C. Increased Likelihood of Heat-Induced Large Wildfires in the Mediterranean Basin. *Sci. Rep.* **2020**, *10*, 13790.

(7) Goss, M.; Swain, D. L.; Abatzoglou, J. T.; Sarhadi, A.; Kolden, C. A.; Williams, A. P.; Diffenbaugh, N. S. Climate Change Is Increasing the Likelihood of Extreme Autumn Wildfire Conditions across California. *Environ. Res. Lett.* **2020**, *15*, 094016.

(8) Caldwell, P. V.; Miniat, C. F.; Elliott, K. J.; Swank, W. T.; Brantley, S. T.; Laseter, S. H. Declining Water Yield from Forested Mountain Watersheds in Response to Climate Change and Forest Mesophication. *Glob. Chang. Biol.* **2016**, *22*, 2997−3012.

(9) Ball, G.; Regier, P.; González-Pinzón, R.; Reale, J.; Van Horn, D. Wildfires Increasingly Impact Western US Fluvial Networks. *Nat. Commun.* **2021**, *12*, 1−8.

(10) Hallema, D. W.; Robinne, F. N.; Bladon, K. D. Reframing the Challenge of Global Wildfire Threats to Water Supplies. *Earth's Future* **2018**, *6*, 772−776.

(11) Clifton, C. F.; Forest, U. N.; Roby, K. B.; Forest, L. N.; Contributors, M.; Hansen, W.; Forest, F. M. N.; Hays, P. E.; Mountain, R.; Office, R.; Connor, A.; Forest, C. N.; Leonard, M.; Forest, P. N. Water, Climate Change, and Forests: Watershed Stewardship for a Changing Climate. *Forest Management for Resilience, Adaptation & Watershed Protection*; Nova Science Publishers, 2012; pp 35−145.

(12) Coogan, S. C. P.; Robinne, F.-N.; Jain, P.; Flannigan, M. D. Scientists' warning on wildfire - a Canadian perspective. *Can. J. For. Res.* **2019**, *49*, 1015−1023.

(13) Price, D. T.; Alfaro, R. I.; Brown, K. J.; Flannigan, M. D.; Fleming, R. A.; Hogg, E. H.; Girardin, M. P.; Lakusta, T.; Johnston, M.; McKenney, D. W.; Pedlar, J. H.; Stratton, T.; Sturrock, R. N.; Thompson, I. D.; Trofymow, J. A.; Venier, L. A. Anticipating the consequences of climate change for Canada's boreal forest ecosystems. *Environ. Rev.* **2013**, *21*, 322−365.
(14) Liu, Y.; Stanturf, J.; Goodrick, S. Trends in Global Wildfire Potential in a Changing Climate. *For. Ecol. Manage.* **2010**, *259*, 685−697.
(15) Pellegrini, A. F. A.; Ahlström, A.; Hobbie, S. E.; Reich, P. B.; Nieradzik, L. P.; Staver, A. C.; Scharenbroch, B. C.; Jumpponen, A.; Anderegg, W. R. L.; Randerson, J. T.; Jackson, R. B. Fire Frequency Drives Decadal Changes in Soil Carbon and Nitrogen and Ecosystem Productivity. *Nature* **2018**, *553*, 194−198.
(16) Caon, L.; Vallejo, V. R.; Ritsema, C. J.; Geissen, V. Effects of Wildfire on Soil Nutrients in Mediterranean Ecosystems. *Earth-Science Rev.* **2014**, *139*, 47−58.
(17) Mataix-Solera, J.; Cerdà, A.; Arcenegui, V.; Jordán, A.; Zavala, L. M. Fire Effects on Soil Aggregation: A Review. *Earth-Science Rev.* **2011**, *109*, 44−60.
(18) Smith, H. G.; Sheridan, G. J.; Lane, P. N. J.; Nyman, P.; Haydon, S. Wildfire Effects on Water Quality in Forest Catchments: A Review with Implications for Water Supply. *J. Hydrol.* **2011**, *396*, 170−192.
(19) De La Rosa, J. M.; González-Pérez, J. A.; González-Vila, F. J.; Knicker, H. Medium Term Effects of Fire Induced Soil Organic Matter Alterations on Andosols under Canarian Pine (Pinus Canariensis). *J. Anal. Appl. Pyrolysis* **2013**, *104*, 269−279.
(20) Pereira, P.; Úbeda, X.; Martin, D. A. Fire Severity Effects on Ash Chemical Composition and Water-Extractable Elements. *Geoderma* **2012**, *191*, 105−114.
(21) D'Andrilli, J.; Junker, J. R.; Smith, H. J.; Scholl, E. A.; Foreman, C. M. DOM Composition Alters Ecosystem Function during Microbial Processing of Isolated Sources. *Biogeochemistry* **2019**, *142*, 281−298.
(22) Hernández, T.; García, C.; Reinhardt, I. Short-Term Effect of Wildfire on the Chemical, Biochemical and Microbiological Properties of Mediterranean Pine Forest Soils. *Biol. Fertil. Soils* **1997**, *25*, 109−116.
(23) LeBauer, D. S.; Treseder, K. K. Nitrogen Limitation of Net Primary Productivity in Terrestrial Ecosystems Is Globally Distributed. *Ecology* **2008**, *89*, 371−379.
(24) Hunt, A. P.; Parry, J. D.; Hamilton-Taylor, J. Further Evidence of Elemental Composition as an Indicator of the Bioavailability of Humic Substances to Bacteria. *Limnol. Oceanogr.* **2000**, *45*, 237−241.
(25) Wiegner, T. N.; Seitzinger, S. P. Seasonal bioavailability of dissolved organic carbon and nitrogen from pristine and polluted freshwater wetlands. *Limnol. Oceanogr.* **2004**, *49*, 1703−1712.
(26) Neary, D. G.; Klopatek, C. C.; DeBano, L. F.; Ffolliott, P. F. Fire Effects on Belowground Sustainability: A Review and Synthesis. *For. Ecol. Manage.* **1999**, *122*, 51−71.
(27) Young, R.; Avneri-Katz, S.; McKenna, A.; Chen, H.; Bahureksa, W.; Polubesova, T.; Chefetz, B.; Borch, T. Composition-Dependent Sorptive Fractionation of Anthropogenic Dissolved Organic Matter by Fe(III)-Montmorillonite. *Soil Syst.* **2018**, *2*, 14.
(28) Scott, E. E.; Rothstein, D. E. The Dynamic Exchange of Dissolved Organic Matter Percolating through Six Diverse Soils. *Soil Biol. Biochem.* **2014**, *69*, 83−92.
(29) Ding, Y.; Watanabe, A.; Jaffé, R. Dissolved Black Nitrogen (DBN) in Freshwater Environments. *Org. Geochem.* **2014**, *68*, 1−4.
(30) Smith, C. R.; Buzan, E. M.; Lee, J. W. Potential Impact of Biochar Water-Extractable Substances on Environmental Sustainability. *ACS Sustainable Chem. Eng.* **2013**, *1*, 118−126.
(31) Hohner, A. K.; Terry, L. G.; Townsend, E. B.; Summers, R. S.; Rosario-Ortiz, F. L. Water Treatment Process Evaluation of Wildfire-Affected Sediment Leachates. *Environ. Sci.: Water Res. Technol.* **2017**, *3*, 352−365.
(32) Chow, A. T.; Tsai, K. P.; Fegel, T. S.; Pierson, D. N.; Rhoades, C. C. Lasting Effects of Wildfire on Disinfection By-Product Formation in Forest Catchments. *J. Environ. Qual.* **2019**, *48*, 1826.
(33) Wang, J.-J.; Dahlgren, R. A.; Erşan, M. S.; Karanfil, T.; Chow, A. T. Wildfire Altering Terrestrial Precursors of Disinfection Byproducts in Forest Detritus. *Environ. Sci. Technol.* **2015**, *49*, 5921−5929.
(34) Keeley, J. E. Fire Intensity, Fire Severity and Burn Severity: A Brief Review and Suggested Usage. *Int. J. Wildland Fire* **2009**, *18*, 116−126.
(35) Boon, J. J.; Pastorova, I.; Botto, R. E.; Arisz, P. W. Structural Studies on Cellulose Pyrolysis and Cellulose Chars by PYMS, PYGCMS, FTIR, NMR and by Wet Chemical Techniques. *Biomass Bioenergy* **1994**, *7*, 25−32.
(36) González-Pérez, J. A.; González-Vila, F. J.; Almendros, G.; Knicker, H. The effect of fire on soil organic matter-a review. *Environ. Int.* **2004**, *30*, 855−870.
(37) Knicker, H. How Does Fire Affect the Nature and Stability of Soil Organic Nitrogen and Carbon? A Review. *Biogeochemistry* **2007**, *85*, 91−118.
(38) Santín, C.; Doerr, S. H.; Kane, E. S.; Masiello, C. A.; Ohlson, M.; de la Rosa, J. M.; Preston, C. M.; Dittmar, T. Towards a Global Assessment of Pyrogenic Carbon from Vegetation Fires. *Glob. Chang. Biol.* **2016**, *22*, 76−91.
(39) Bird, M. I.; Wynn, J. G.; Saiz, G.; Wurster, C. M.; McBeath, A. The Pyrogenic Carbon Cycle. *Annu. Rev. Earth Planet. Sci.* **2015**, *43*, 273−298.
(40) Wagner, S.; Jaffé, R.; Stubbins, A. Dissolved Black Carbon in Aquatic Ecosystems. *Limnol. Oceanogr. Lett.* **2018**, *3*, 168−185.
(41) Baldock, J. A.; Smernik, R. J. Chemical Composition and Bioavailability of Thermally Altered Pinus Resinosa (Red Pine) Wood. *Org. Geochem.* **2002**, *33*, 1093−1109.
(42) Knicker, H. "Black nitrogen"—an important fraction in determining the recalcitrance of charcoal. *Org. Geochem.* **2010**, *41*, 947−950.
(43) Knicker, H.; Hilscher, A.; González-Vila, F. J.; Almendros, G. A New Conceptual Model for the Structural Properties of Char Produced during Vegetation Fires. *Org. Geochem.* **2008**, *39*, 935−939.
(44) Wan, X.; Kawamura, K.; Ram, K.; Kang, S.; Loewen, M.; Gao, S.; Wu, G.; Fu, P.; Zhang, Y.; Bhattarai, H.; Cong, Z. Aromatic Acids as Biomass-Burning Tracers in Atmospheric Aerosols and Ice Cores: A Review. *Environ. Pollut.* **2019**, *247*, 216−228.
(45) De la Rosa, J. M.; Faria, S. R.; Varela, M. E.; Knicker, H.; González-Vila, F. J.; González-Pérez, J. A.; Keizer, J. Characterization of Wildfire Effects on Soil Organic Matter Using Analytical Pyrolysis. *Geoderma* **2012**, *191*, 24−30.
(46) Almendros, G.; Tinoco, P.; De la Rosa, J.-M.; Knicker, H.; González-Pérez, J.-A.; González-Vila, F. J. Selective Effects of Forest Fires on the Structural Domains of Soil Humic Acids as Shown by Dipolar Dephasing 13C NMR and Graphical-Statistical Analysis of Pyrolysis Compounds. *J. Soils Sediments* **2016**, *18*, 1303−1313.
(47) Campo, J.; Nierop, K. G. J.; Cammeraat, E.; Andreu, V.; Rubio, J. L. Application of Pyrolysis-Gas Chromatography/Mass Spectrometry to Study Changes in the Organic Matter of Macro- and Microaggregates of a Mediterranean Soil upon Heating. *J. Chromatogr. A* **2011**, *1218*, 4817−4827.
(48) Chen, H.; Rhoades, C. C.; Chow, A. T. Characteristics of Soil Organic Matter 14 Years after a Wildfire: A Pyrolysis-Gas-Chromatography Mass Spectrometry (Py-GC-MS) Study. *J. Anal. Appl. Pyrolysis* **2020**, *152*, 104922.
(49) Knicker, H.; Gonzalezvila, F.; Polvillo, O.; Gonzalez, J.; Almendros, G. Fire-Induced Transformation of C- and N- Forms in Different Organic Soil Fractions from a Dystric Cambisol under a Mediterranean Pine Forest (Pinus Pinaster). *Soil Biol. Biochem.* **2005**, *37*, 701−718.
(50) Otto, A.; Gondokusumo, R.; Simpson, M. J. Characterization and Quantification of Biomarkers from Biomass Burning at a Recent Wildfire Site in Northern Alberta, Canada. *Appl. Geochem.* **2006**, *21*, 166−183.

https://doi.org/10.1021/acs.est.1c06745
Environ. Sci. Technol. 2022, 56, 4597−4609

(51) Sazawa, K.; Yoshida, H.; Okusu, K.; Hata, N.; Kuramitz, H. Effects of Forest Fire on the Properties of Soil and Humic Substances Extracted from Forest Soil in Gunma, Japan. *Environ. Sci. Pollut. Res.* **2018**, *25*, 30325−30338.
(52) Orasche, J.; Schnelle-Kreis, J.; Abbaszade, G.; Zimmermann, R. Technical Note: In-Situ Derivatization Thermal Desorption GC-TOFMS for Direct Analysis of Particle-Bound Non-Polar and Polar Organic Species. *Atmos. Chem. Phys.* **2011**, *11*, 8977−8993.
(53) Piot, C.; Jaffrezo, J.-L.; Cozic, J.; Pissot, N.; El Haddad, I.; Marchand, N.; Besombes, J.-L. Quantification of levoglucosan and its isomers by High Performance Liquid Chromatography - Electrospray Ionization tandem Mass Spectrometry and its applications to atmospheric and soil samples. *Atmos. Meas. Tech.* **2012**, *5*, 141−148.
(54) Hoffmann, D.; Iinuma, Y.; Herrmann, H. Development of a Method for Fast Analysis of Phenolic Molecular Markers in Biomass Burning Particles Using High Performance Liquid Chromatography/Atmospheric Pressure Chemical Ionisation Mass Spectrometry. *J. Chromatogr. A* **2007**, *1143*, 168−175.
(55) Maie, N.; Knicker, H.; Watanabe, A.; Kimura, M. Heterocyclic N in the Highly Humified Humic Acids Extracted from the Subsoil of Paddy Fields and Surface Ando Soils. *Org. Geochem.* **2006**, *37*, 12−19.
(56) Maie, N.; Parish, K. J.; Watanabe, A.; Knicker, H.; Benner, R.; Abe, T.; Kaiser, K.; Jaffé, R. Chemical Characteristics of Dissolved Organic Nitrogen in an Oligotrophic Subtropical Coastal Ecosystem. *Geochim. Cosmochim. Acta* **2006**, *70*, 4491−4506.
(57) de Oliveira, F. C.; Coimbra, J. S. d. R.; de Oliveira, E. B.; Zuñiga, A. D. G.; Rojas, E. E. G. Food Protein-Polysaccharide Conjugates Obtained via the Maillard Reaction: A Review. *Crit. Rev. Food Sci. Nutr.* **2016**, *56*, 1108−1125.
(58) Knicker, H. Soil Organic N - An under-Rated Player for C Sequestration in Soils? *Soil Biol. Biochem.* **2011**, *43*, 1118−1129.
(59) Knicker, H. Stabilization of N-compounds in soil and organic-matter-rich sediments-what is the difference? *Mar. Chem.* **2004**, *92*, 167−195.
(60) Almendros, G.; Knicker, H.; González-Vila, F. J. Rearrangement of Carbon and Nitrogen Forms in Peat after Progressive Thermal Oxidation as Determined by Solid-State 13C- and 15N-NMR Spectroscopy. *Org. Geochem.* **2003**, *34*, 1559−1568.
(61) Jiménez-Morillo, N. T.; González-Pérez, J. A.; Almendros, G.; De La Rosa, J. M.; Waggoner, D. C.; Jordán, A.; Zavala, L. M.; González-Vila, F. J.; Hatcher, P. G. Ultra-High Resolution Mass Spectrometry of Physical Speciation Patterns of Organic Matter in Fire-Affected Soils. *J. Environ. Manage.* **2018**, *225*, 139−147.
(62) De la Rosa, J. M.; Knicker, H. Bioavailability of N Released from N-Rich Pyrogenic Organic Matter: An Incubation Study. *Soil Biol. Biochem.* **2011**, *43*, 2368−2373.
(63) Hilscher, A.; Knicker, H. Carbon and Nitrogen Degradation on Molecular Scale of Grass-Derived Pyrogenic Organic Material during 28 Months of Incubation in Soil. *Soil Biol. Biochem.* **2011**, *43*, 261−270.
(64) Bahureksa, W.; Tfaily, M. M.; Boiteau, R. M.; Young, R. B.; Logan, M. N.; McKenna, A. M.; Borch, T.; Young, R. B.; Logan, M. N.; Borch, T. Soil Organic Matter Characterization by Fourier Transform Ion Cyclotron Resonance Mass Spectrometry (FTICR MS): A Critical Review of Sample Preparation, Analysis, and Data Interpretation. *Environ. Sci. Technol.* **2021**, *55*, 9637−9656.
(65) Cho, Y.; Ahmed, A.; Islam, A.; Kim, S. Developments in FT-ICR Ms Instrumentation, Ionization Techniques, and Data Interpretation Methods for Petroleomics. *Mass Spectrom. Rev.* **2015**, *34*, 248−263.
(66) Matilainen, A.; Gjessing, E. T.; Lahtinen, T.; Hed, L.; Bhatnagar, A.; Sillanpää, M. An Overview of the Methods Used in the Characterisation of Natural Organic Matter (NOM) in Relation to Drinking Water Treatment. *Chemosphere* **2011**, *83*, 1431−1442.
(67) Nebbioso, A.; Piccolo, A. Molecular Characterization of Dissolved Organic Matter (DOM): A Critical Review. *Anal. Bioanal. Chem.* **2013**, *405*, 109−124.
(68) Sleighter, R. L.; Hatcher, P. G. The Application of Electrospray Ionization Coupled to Ultrahigh Resolution Mass Spectrometry for the Molecular Characterization of Natural Organic Matter. *J. Mass Spectrom.* **2007**, *42*, 559−574.
(69) Li, Y.; Harir, M.; Uhl, J.; Kanawati, B.; Lucio, M.; Smirnov, K. S.; Koch, B. P.; Schmitt-Kopplin, P.; Hertkorn, N. How Representative Are Dissolved Organic Matter (DOM) Extracts? A Comprehensive Study of Sorbent Selectivity for DOM Isolation. *Water Res.* **2017**, *116*, 316−323.
(70) Roth, V.-N.; Lange, M.; Simon, C.; Hertkorn, N.; Bucher, S.; Goodall, T.; Griffiths, R. I.; Mellado-Vázquez, P. G.; Mommer, L.; Oram, N. J.; Weigelt, A.; Dittmar, T.; Gleixner, G. Persistence of Dissolved Organic Matter Explained by Molecular Changes during Its Passage through Soil. *Nat. Geosci.* **2019**, *12*, 755−761.
(71) Ohno, T.; Parr, T. B.; Gruselle, M. C. I.; Fernandez, I. J.; Sleighter, R. L.; Hatcher, P. G. Molecular Composition and Biodegradability of Soil Organic Matter: A Case Study Comparing Two New England Forest Types. *Environ. Sci. Technol.* **2014**, *48*, 7229−7236.
(72) Malik, A. A.; Roth, V.-N.; Hébert, M.; Tremblay, L.; Dittmar, T.; Gleixner, G. Linking Molecular Size, Composition and Carbon Turnover of Extractable Soil Microbial Compounds. *Soil Biol. Biochem.* **2016**, *100*, 66−73.
(73) Romero, C. M.; Engel, R. E.; D'Andrilli, J.; Chen, C.; Zabinski, C.; Miller, P. R.; Wallander, R. Patterns of Change in Permanganate Oxidizable Soil Organic Matter from Semiarid Drylands Reflected by Absorbance Spectroscopy and Fourier Transform Ion Cyclotron Resonance Mass Spectrometry. *Org. Geochem.* **2018**, *120*, 19−30.
(74) Tfaily, M. M.; Chu, R. K.; Tolić, N.; Roscioli, K. M.; Anderton, C. R.; Paša-Tolić, L.; Robinson, E. W.; Hess, N. J. Advanced Solvent Based Methods for Molecular Characterization of Soil Organic Matter by High-Resolution Mass Spectrometry. *Anal. Chem.* **2015**, *87*, 5206−5215.
(75) O'Donnell, J. A.; Aiken, G. R.; Butler, K. D.; Guillemette, F.; Podgorski, D. C.; Spencer, R. G. M. DOM composition and transformation in boreal forest soils: The effects of temperature and organic-horizon decomposition state. *J. Geophys. Res.: Biogeosci.* **2016**, *121*, 2727−2744.
(76) Patel, K. F.; Tejnecký, V.; Ohno, T.; Bailey, V. L.; Sleighter, R. L.; Hatcher, P. G. Reactive Oxygen Species Alter Chemical Composition and Adsorptive Fractionation of Soil-Derived Organic Matter. *Geoderma* **2021**, *384*, 114805.
(77) Gonsior, M.; Zwartjes, M.; Cooper, W. J.; Song, W.; Ishida, K. P.; Tseng, L. Y.; Jeung, M. K.; Rosso, D.; Hertkorn, N.; Schmitt-Kopplin, P. Molecular Characterization of Effluent Organic Matter Identified by Ultrahigh Resolution Mass Spectrometry. *Water Res.* **2011**, *45*, 2943−2953.
(78) Flerus, R.; Koch, B. P.; Schmitt-Kopplin, P.; Witt, M.; Kattner, G. Molecular Level Investigation of Reactions between Dissolved Organic Matter and Extraction Solvents Using FT-ICR MS. *Mar. Chem.* **2011**, *124*, 100−107.
(79) Hertkorn, N.; Frommberger, M.; Witt, M.; Koch, B. P.; Schmitt-Kopplin, P.; Perdue, E. M.; Hertkorn, N.; Frommberger, M.; Witt, M.; Koch, B. P.; Schmitt-Kopplin, P. Natural Organic Matter and the Event Horizon of Mass Spectrometry. *Anal. Chem.* **2008**, *80*, 8908−8919.
(80) Li, Y.; Harir, M.; Lucio, M.; Kanawati, B.; Smirnov, K.; Flerus, R.; Koch, B. P.; Schmitt-Kopplin, P.; Hertkorn, N. Proposed Guidelines for Solid Phase Extraction of Suwannee River Dissolved Organic Matter. *Anal. Chem.* **2016**, *88*, 6680−6688.
(81) Hertkorn, N.; Harir, M.; Cawley, K. M.; Schmitt-Kopplin, P.; Jaffé, R. Molecular Characterization of Dissolved Organic Matter from Subtropical Wetlands: A Comparative Study through the Analysis of Optical Properties, NMR and FTICR/MS. *Biogeosciences* **2016**, *13*, 2257−2277.
(82) Koch, B. P.; Ludwichowski, K.-U.; Kattner, G.; Dittmar, T.; Witt, M. Advanced Characterization of Marine Dissolved Organic Matter by Combining Reversed-Phase Liquid Chromatography and FT-ICR-MS. *Mar. Chem.* **2008**, *111*, 233−241.
(83) Wagner, S.; Riedel, T.; Niggemann, J.; Vähätalo, A. V.; Dittmar, T.; Jaffé, R. Linking the Molecular Signature of Heteroatomic

https://doi.org/10.1021/acs.est.1c06745
Environ. Sci. Technol. 2022, 56, 4597−4609

Dissolved Organic Matter to Watershed Characteristics in World Rivers. *Environ. Sci. Technol.* **2015**, *49*, 13798−13806.
(84) Kellerman, A. M.; Kothawala, D. N.; Dittmar, T.; Tranvik, L. J. Persistence of Dissolved Organic Matter in Lakes Related to Its Molecular Characteristics. *Nat. Geosci.* **2015**, *8*, 454−457.
(85) Riedel, T.; Zark, M.; Vähätalo, A. V.; Niggemann, J.; Spencer, R. G. M.; Hernes, P. J.; Dittmar, T. Molecular Signatures of Biogeochemical Transformations in Dissolved Organic Matter from Ten World Rivers. *Front. Earth Sci.* **2016**, *4*, 1−16.
(86) Fox, P. M.; Nico, P. S.; Tfaily, M. M.; Heckman, K.; Davis, J. A. Characterization of Natural Organic Matter in Low-Carbon Sediments: Extraction and Analytical Approaches. *Org. Geochem.* **2017**, *114*, 12−22.
(87) Podgorski, D. C.; Hamdan, R.; McKenna, A. M.; Nyadong, L.; Rodgers, R. P.; Marshall, A. G.; Cooper, W. T. Characterization of Pyrogenic Black Carbon by Desorption Atmospheric Pressure Photoionization Fourier Transform Ion Cyclotron Resonance Mass Spectrometry. *Anal. Chem.* **2012**, *84*, 1281−1287.
(88) Wagner, S.; Dittmar, T.; Jaffé, R. Molecular Characterization of Dissolved Black Nitrogen via Electrospray Ionization Fourier Transform Ion Cyclotron Resonance Mass Spectrometry. *Org. Geochem.* **2015**, *79*, 21−30.
(89) Smith, C. R.; Sleighter, R. L.; Hatcher, P. G.; Lee, J. W. Molecular Characterization of Inhibiting Biochar Water-Extractable Substances Using Electrospray Ionization Fourier Transform Ion Cyclotron Resonance Mass Spectrometry. *Environ. Sci. Technol.* **2013**, *47*, 13294−13302.
(90) Kramer, R. W.; Kujawinski, E. B.; Hatcher, P. G. Identification of Black Carbon Derived Structures in a Volcanic Ash Soil Humic Acid by Fourier Transform Ion Cyclotron Resonance Mass Spectrometry. *Environ. Sci. Technol.* **2004**, *38*, 3387−3395.
(91) Song, J.; Li, M.; Fan, X.; Zou, C.; Zhu, M.; Jiang, B.; Yu, Z.; Jia, W.; Liao, Y.; Peng, P. a. Molecular Characterization of Water- And Methanol-Soluble Organic Compounds Emitted from Residential Coal Combustion Using Ultrahigh-Resolution Electrospray Ionization Fourier Transform Ion Cyclotron Resonance Mass Spectrometry. *Environ. Sci. Technol.* **2019**, *53*, 13607−13617.
(92) Solihat, N. N.; Yustiawati; Kim, S.; Kim, S. Elucidating Molecular Level Impact of Peat Fire on Soil Organic Matter by Laser Desorption Ionization Fourier Transform Ion Cyclotron Resonance Mass Spectrometry. *Anal. Bioanal. Chem.* **2019**, *411*, 7303−7313.
(93) Wozniak, A. S.; Goranov, A. I.; Mitra, S.; Bostick, K. W.; Zimmerman, A. R.; Schlesinger, D. R.; Myneni, S.; Hatcher, P. G. Molecular Heterogeneity in Pyrogenic Dissolved Organic Matter from a Thermal Series of Oak and Grass Chars. *Org. Geochem.* **2020**, *148*, 104065.
(94) Chen, H.; Tsai, K.-P.; Liu, Y.; Tolić, N.; Burton, S. D.; Chu, R.; Karanfil, T.; Chow, A. T. Characterization of Dissolved Organic Matter from Wildfire-Induced Microcystis Aeruginosa Blooms Controlled by Copper Sulfate as Disinfection Byproduct Precursors Using APPI(-) and ESI(-) FT-ICR MS. *Water Res.* **2021**, *189*, 116640.
(95) McKenna, A. M.; Marshall, A. G.; Rodgers, R. P. Heavy Petroleum Composition. 4. Asphaltene Compositional Space. *Energy Fuels* **2013**, *27*, 1257−1267.
(96) McKenna, A. M.; Donald, L. J.; Fitzsimmons, J. E.; Juyal, P.; Spicer, V.; Standing, K. G.; Marshall, A. G.; Rodgers, R. P. Heavy Petroleum Composition. 3. Asphaltene Aggregation. *Energy Fuels* **2013**, *27*, 1246−1256.
(97) Purcell, J. M.; Hendrickson, C. L.; Rodgers, R. P.; Marshall, A. G. Atmospheric Pressure Photoionization Fourier Transform Ion Cyclotron Resonance Mass Spectrometry for Complex Mixture Analysis. *Anal. Chem.* **2006**, *78*, 5906−5912.
(98) Niles, S. F.; Chacón-Patiño, M. L.; Smith, D. F.; Rodgers, R. P.; Marshall, A. G. Comprehensive Compositional and Structural Comparison of Coal and Petroleum Asphaltenes Based on Extrography Fractionation Coupled with Fourier Transform Ion Cyclotron Resonance MS and MS/MS Analysis. *Energy Fuels* **2020**, *34*, 1492−1505.
(99) Lobodin, V. V.; Juyal, P.; McKenna, A. M.; Rodgers, R. P.; Marshall, A. G. Silver Cationization for Rapid Speciation of Sulfur-Containing Species in Crude Oils by Positive Electrospray Ionization Fourier Transform Ion Cyclotron Resonance Mass Spectrometry. *Energy Fuels* **2014**, *28*, 447−452.
(100) Jarvis, J. M.; McKenna, A. M.; Hilten, R. N.; Das, K. C.; Rodgers, R. P.; Marshall, A. G. Characterization of Pine Pellet and Peanut Hull Pyrolysis Bio-Oils by Negative-Ion Electrospray Ionization Fourier Transform Ion Cyclotron Resonance Mass Spectrometry. *Energy Fuels* **2012**, *26*, 3810−3815.
(101) Marshall, A. G.; Hendrickson, C. L.; Jackson, G. S. Fourier Transform Ion Cyclotron Resonance Mass Spectrometry: A Primer. *Mass Spectrom. Rev.* **1998**, *17*, 1−35.
(102) Hohner, A. K.; Cawley, K.; Oropeza, J.; Summers, R. S.; Rosario-Ortiz, F. L. Drinking Water Treatment Response Following a Colorado Wildfire. *Water Res.* **2016**, *105*, 187−198.
(103) Zark, M.; Dittmar, T. Universal Molecular Structures in Natural Dissolved Organic Matter. *Nat. Commun.* **2018**, *9*, 1−8.
(104) Wagner, S.; Ding, Y.; Jaffé, R. A New Perspective on the Apparent Solubility of Dissolved Black Carbon. *Front. Earth Sci.* **2017**, *5*, 75.
(105) Hohner, A. K.; Rhoades, C. C.; Wilkerson, P.; Rosario-Ortiz, F. L. Wildfires Alter Forest Watersheds and Threaten Drinking Water Quality. *Acc. Chem. Res.* **2019**, *52*, 1234−1244.
(106) Thurman, E. M.; Yu, Y.; Ferrer, I.; Thorn, K. A.; Rosario-Ortiz, F. L. Molecular Identification of Water-Extractable Organic Carbon from Thermally Heated Soils: C-13 NMR and Accurate Mass Analyses Find Benzene and Pyridine Carboxylic Acids. *Environ. Sci. Technol.* **2020**, *54*, 2994−3001.
(107) Dunn, P. H.; Barro, S. C.; Poth, M. Soil Moisture Affects Survival Of Microorganisms In Heated Chaparral Soil. *Soil Biol. Biochem.* **1985**, *17*, 143−148.
(108) Emmett, M. R.; White, F. M.; Hendrickson, C. L.; Shi, S. D.-H.; Marshall, A. G. Application of Micro-Electrospray Liquid Chromatography Techniques to FT-ICR MS to Enable High-Sensitivity Biological Analysis. *J. Am. Soc. Mass Spectrom.* **1998**, *9*, 333−340.
(109) Kaiser, N. K.; Quinn, J. P.; Blakney, G. T.; Hendrickson, C. L.; Marshall, A. G. A Novel 9.4 Tesla FTICR Mass Spectrometer with Improved Sensitivity, Mass Resolution, and Mass Range. *J. Am. Soc. Mass Spectrom.* **2011**, *22*, 1343−1351.
(110) Savory, J. J.; Kaiser, N. K.; McKenna, A. M.; Xian, F.; Blakney, G. T.; Rodgers, R. P.; Hendrickson, C. L.; Marshall, A. G. Parts-Per-Billion Fourier Transform Ion Cyclotron Resonance Mass Measurement Accuracy with a "Walking" Calibration Equation. *Anal. Chem.* **2011**, *83*, 1732−1736.
(111) Kendrick, E. A Mass Scale Based on CH2 = 14.0000 for High Resolution Mass Spectrometry of Organic Compounds. *Anal. Chem.* **1963**, *35*, 2146−2154.
(112) Hughey, C. A.; Hendrickson, C. L.; Rodgers, R. P.; Marshall, A. G.; Qian, K. Kendrick Mass Defect Spectrum: A Compact Visual Analysis for Ultrahigh-Resolution Broadband Mass Spectra. *Anal. Chem.* **2001**, *73*, 4676−4681.
(113) Corilo, Y. E. *PetroOrg Software*; Florida State University, Omics LLC: Tallahassee, Fl, 2014.
(114) Vetter, W. F. W. McLafferty, F. Turecek. Interpretation of mass spectra. Fourth edition (1993). University Science Books, Mill Valley, California. *Biol. Mass Spectrom.* **1994**, *23*, 379.
(115) Kind, T.; Fiehn, O. Seven Golden Rules for Heuristic Filtering of Molecular Formulas Obtained by Accurate Mass Spectrometry. *BMC Bioinf.* **2007**, *8*, 105.
(116) Koch, B. P.; Dittmar, T. From Mass to Structure: An Aromaticity Index for High-Resolution Mass Data of Natural Organic Matter. *Rapid Commun. Mass Spectrom.* **2006**, *20*, 926−932.
(117) Melendez-Perez, J. J.; Martínez-Mejia, M. J.; Eberlin, M. N. A Reformulated Aromaticity Index Equation under Consideration for Non-Aromatic and Non-Condensed Aromatic Cyclic Carbonyl Compounds. *Org. Geochem.* **2016**, *95*, 29−33.

https://doi.org/10.1021/acs.est.1c06745
Environ. Sci. Technol. 2022, 56, 4597−4609

(118) Ferrer, I.; Thurman, E. M.; Zweigenbaum, J. A.; Murphy, S. F.; Webster, J. P.; Rosario-Ortiz, F. L. Wildfires: Identification of a New Suite of Aromatic Polycarboxylic Acids in Ash and Surface Water. *Sci. Total Environ.* **2021**, *770*, 144661.
(119) Chen, M.; Kim, S.; Park, J.-E.; Kim, H. S.; Hur, J. Effects of Dissolved Organic Matter (DOM) Sources and Nature of Solid Extraction Sorbent on Recoverable DOM Composition: Implication into Potential Lability of Different Compound Groups. *Anal. Bioanal. Chem.* **2016**, *408*, 4809−4819.
(120) Tfaily, M. M.; Hodgkins, S.; Podgorski, D. C.; Chanton, J. P.; Cooper, W. T. Comparison of Dialysis and Solid-Phase Extraction for Isolation and Concentration of Dissolved Organic Matter Prior to Fourier Transform Ion Cyclotron Resonance Mass Spectrometry. *Anal. Bioanal. Chem.* **2012**, *404*, 447−457.
(121) Sharma, R. K.; Wooten, J. B.; Baliga, V. L.; Hajaligol, M. R. Characterization of Chars from Biomass-Derived Materials: Pectin Chars. *Fuel* **2001**, *80*, 1825−1836.
(122) Smuda, M.; Glomb, M. A. Fragmentation Pathways during Maillard-Induced Carbohydrate Degradation. *J. Agric. Food Chem.* **2013**, *61*, 10198−10208.
(123) Weenen, H. Reactive Intermediates and Carbohydrate Fragmentation in Maillard Chemistry. *Food Chem.* **1998**, *62*, 393−401.
(124) Elmore, J. S.; Mottram, D. S. Investigation of the Reaction between Ammonium Sulfide, Aldehydes, and α-Hydroxyketones or α-Dicarbonyls To Form Some Lipid−Maillard Interaction Products Found in Cooked Beef. *J. Agric. Food Chem.* **1997**, *45*, 3595−3602.
(125) Henning, C.; Glomb, M. A. Pathways of the Maillard Reaction under Physiological Conditions. *Glycoconjugate J.* **2016**, *33*, 499−512.
(126) Hemmler, D.; Roullier-Gall, C.; Marshall, J. W.; Rychlik, M.; Taylor, A. J.; Schmitt-Kopplin, P. Evolution of Complex Maillard Chemical Reactions, Resolved in Time. *Sci. Rep.* **2017**, *7*, 3227.
(127) Vranova, V.; Zahradnickova, H.; Janous, D.; Skene, K. R.; Matharu, A. S.; Rejsek, K.; Formanek, P. The Significance of D-Amino Acids in Soil, Fate and Utilization by Microbes and Plants: Review and Identification of Knowledge Gaps. *Plant Soil* **2012**, *354*, 21−39.
(128) Liang, C.; Amelung, W.; Lehmann, J.; Kästner, M. Quantitative Assessment of Microbial Necromass Contribution to Soil Organic Matter. *Glob. Chang. Biol.* **2019**, *25*, 3578−3590.
(129) Moe, L. A. Amino Acids in the Rhizosphere: From Plants to Microbes. *Am. J. Bot.* **2013**, *100*, 1692−1705.
(130) Miltner, A.; Bombach, P.; Schmidt-Brücken, B.; Kästner, M. SOM Genesis: Microbial Biomass as a Significant Source. *Biogeochemistry* **2012**, *111*, 41−55.
(131) Liang, C.; Kästner, M.; Joergensen, R. G. Microbial Necromass on the Rise: The Growing Focus on Its Role in Soil Organic Matter Development. *Soil Biol. Biochem.* **2020**, *150*, 108000.
(132) Lund, M. N.; Ray, C. A. Control of Maillard Reactions in Foods: Strategies and Chemical Mechanisms. *J. Agric. Food Chem.* **2017**, *65*, 4537−4552.
(133) Hestrin, R.; Torres-Rojas, D.; Dynes, J. J.; Hook, J. M.; Regier, T. Z.; Gillespie, A. W.; Smernik, R. J.; Lehmann, J. Fire-Derived Organic Matter Retains Ammonia through Covalent Bond Formation. *Nat. Commun.* **2019**, *10*, 664.
(134) Prieto-Fernández, Á.; Carballas, M.; Carballas, T. Inorganic and Organic N Pools in Soils Burned or Heated: Immediate Alterations and Evolution after Forest Wildfires. *Geoderma* **2004**, *121*, 291−306.
(135) Yaylayan, V. Classification of the Maillard Reaction. A Conceptual Approach. *Trends Food Sci. Technol.* **1997**, *81*, 13−18.
(136) Hemmler, D.; Roullier-Gall, C.; Marshall, J. W.; Rychlik, M.; Taylor, A. J.; Schmitt-Kopplin, P. Insights into the Chemistry of Non-Enzymatic Browning Reactions in Different Ribose-Amino Acid Model Systems. *Sci. Rep.* **2018**, *8*, 16879.
(137) Spencer, C. N.; Gabel, K. O.; Hauer, F. R. Wildfire Effects on Stream Food Webs and Nutrient Dynamics in Glacier National Park, USA. *For. Ecol. Manage.* **2003**, *178*, 141−153.
(138) Roth, V.-N.; Dittmar, T.; Gaupp, R.; Gleixner, G. The Molecular Composition of Dissolved Organic Matter in Forest Soils as a Function of PH and Temperature. *PLoS One* **2015**, *10*, No. e0119188.
(139) Bostick, K. W.; Zimmerman, A. R.; Goranov, A. I.; Mitra, S.; Hatcher, P. G.; Wozniak, A. S. Biolability of Fresh and Photodegraded Pyrogenic Dissolved Organic Matter From Laboratory-Prepared Chars. *J. Geophys. Res.: Biogeosci.* **2021**, *126*, 1−17.
(140) Nelson, A. R.; Narrowe, A. B.; Rhoades, C. C.; Fegel, T. S.; Daly, R. A.; Roth, H. K.; Chu, R. K.; Amundson, K. K.; Geonczy, S. E.; Emerson, J. B.; Young, R. B.; Steindorff, A. S.; Mondo, S. J.; Grigoriev, I. V.; Salamov, A.; Borch, T.; Wilkins, M. J. Playing with FiRE: A Genome Resolved View of the Soil Microbiome Responses to High Severity Forest Wildfire. **2021**, bioRxiv 2021.08.17.456416.
(141) Huang, H.; Wu, Q.-Y.; Hu, H.-Y.; Mitch, W. A. Dichloroacetonitrile and Dichloroacetamide Can Form Independently during Chlorination and Chloramination of Drinking Waters, Model Organic Matters, and Wastewater Effluents. *Environ. Sci. Technol.* **2012**, *46*, 10624−10631.
(142) Yang, X.; Shen, Q.; Guo, W.; Peng, J.; Liang, Y. Precursors and Nitrogen Origins of Trichloronitromethane and Dichloroacetonitrile during Chlorination/Chloramination. *Chemosphere* **2012**, *88*, 25−32.
(143) Chuang, Y.-H.; Tung, H.-h. Formation of Trichloronitromethane and Dichloroacetonitrile in Natural Waters: Precursor Characterization, Kinetics and Interpretation. *J. Hazard. Mater.* **2015**, *283*, 218−226.
(144) Podgorski, D. C.; McKenna, A. M.; Rodgers, R. P.; Marshall, A. G.; Cooper, W. T. Selective Ionization of Dissolved Organic Nitrogen by Positive Ion Atmospheric Pressure Photoionization Coupled with Fourier Transform Ion Cyclotron Resonance Mass Spectrometry. *Anal. Chem.* **2012**, *84*, 5085−5090.
(145) Roth, H. K.; Borch, T.; Young, R. B.; Bahureksa, W.; Blakney, G. T.; Nelson, A. R.; Wilkins, M. J.; McKenna, A. M. Enhanced Speciation of Pyrogenic Organic Matter from Wildfires Enabled by 21 T FT-ICR Mass Spectrometry. *Anal. Chem.* **2022**, *94*, 2973−2980.
(146) Knicker, H.; Almendros, G.; González-Vila, F. J.; Martin, F.; Lüdemann, H.-D. 13C- and 15N-NMR spectroscopic examination of the transformation of organic nitrogen in plant biomass during thermal treatment. *Soil Biol. Biochem.* **1996**, *28*, 1053−1060.
(147) Smith, C. R.; Hatcher, P. G.; Kumar, S.; Lee, J. W. Investigation into the Sources of Biochar Water-Soluble Organic Compounds and Their Potential Toxicity on Aquatic Microorganisms. *ACS Sustainable Chem. Eng.* **2016**, *4*, 2550−2558.

https://doi.org/10.1021/acs.est.1c06745
Environ. Sci. Technol. 2022, 56, 4597−4609